

## Self-sustained nonlinear waves in traffic flow

M. R. Flynn,<sup>1</sup> A. R. Kasimov,<sup>2</sup> J.-C. Nave,<sup>2</sup> R. R. Rosales,<sup>2</sup> and B. Seibold<sup>2</sup><sup>1</sup>*Department of Mechanical Engineering and Applied Mathematics Institute, University of Alberta, Edmonton, Alberta, Canada T6G 2G8*<sup>2</sup>*Department of Mathematics, Massachusetts Institute of Technology,**77 Massachusetts Avenue, Cambridge, Massachusetts 02139, USA*

(Received 16 October 2008; revised manuscript received 5 March 2009; published 26 May 2009)

In analogy to gas-dynamical detonation waves, which consist of a shock with an attached exothermic reaction zone, we consider herein nonlinear traveling wave solutions to the hyperbolic (“inviscid”) continuum traffic equations. Generic existence criteria are examined in the context of the Lax entropy conditions. Our analysis naturally precludes traveling wave solutions for which the shocks travel downstream more rapidly than individual vehicles. Consistent with recent experimental observations from a periodic roadway [Y. Sugiyama *et al.*, *N. J. Phys.* **10**, 033001 (2008)], our numerical calculations show that nonlinear traveling waves are attracting solutions, with the time evolution of the system converging toward a wave-dominated configuration. Theoretical principles are elucidated by considering examples of traffic flow on open and closed roadways.

DOI: [10.1103/PhysRevE.79.056113](https://doi.org/10.1103/PhysRevE.79.056113)

PACS number(s): 89.40.Bb, 47.10.ab, 47.40.Rs

## I. INTRODUCTION AND PROBLEM FORMULATION

The economic costs in terms of lost productivity, atmospheric pollution, and vehicular collisions associated with traffic jams are substantial both in developed and developing nations. As such, the discipline of traffic science has expanded significantly in recent decades, particularly from the point of view of theoretical modeling [1]. Borrowing terminology applied in Payne [2] and elsewhere, three generic categories describe the approaches considered in most previous analyses. “Microscopic” models such as “follow the leader” studies [3] or “optimal velocity” studies [4] consider the individual (i.e., Lagrangian) response of a driver to his or her neighbors, in particular, the vehicle immediately ahead. “Mesoscopic” or “gas-kinetic macroscopic” analyses such as the examinations of Phillips [5] take a statistical mechanics approach in which vehicle interactions are modeled using ideas familiar from kinetic theory. Finally, “macroscopic” studies [2,6–11] model traffic flow using conservation laws and a suitable adaptation of the methods of continuum mechanics [12,13], which yields governing equations similar to those from fluid mechanics. It is this latter category of analysis that is of interest here.

Treating the traffic flow as a continuum, we begin by considering a one-dimensional Payne-Whitham model on either an infinite roadway or, as with the recent physical experiment conducted by Sugiyama *et al.* [14], a closed periodic roadway, say of length  $\lambda$ . The governing equations for mass and momentum read (e.g., Kerner and Konhäuser [9])

$$\rho_t + (\rho u)_x = 0, \quad (1.1)$$

$$u_t + uu_x + \frac{1}{\rho} p_x = \frac{1}{\tau} (\tilde{u} - u), \quad (1.2)$$

where the subscripts indicate differentiation,  $\tau$  is a relaxation time scale,  $u$  is the traffic speed, and  $\rho$  is the traffic density—with units of vehicles/length. The traffic pressure,  $p$ , incorporates the effects of kinematic dispersion and the “preventive” driving needed to compensate for the time delay  $\tau$ ;  $p$  is

typically assumed to be an (increasing) function of the density only, i.e.,  $p=p(\rho)$  [10,15]. Here, in order to have a well-behaved theoretical formulation in the presence of shock waves [16], we shall assume that  $p$  is a convex function of the specific volume  $v=1/\rho$  (road length per vehicle). This implies that  $dp/dv < 0$  and  $d^2p/dv^2 > 0$ , which holds for the functions typically assigned to  $p$  in macroscopic models. Finally,  $\tilde{u}=\tilde{u}(\rho)$  gives, for a particular traffic density, the desired or equilibrium speed to which the drivers try to adjust. The precise functional form of  $\tilde{u}$  is, to a certain degree, rather arbitrary and indeed several variants have been proposed [1]. Generally,  $\tilde{u}$  is a decreasing one-to-one function of the density, with  $0 < \tilde{u}(0) = \tilde{u}_0 < \infty$  and  $\tilde{u}(\rho_M) = 0$ , where (i)  $\rho_M$  denotes the maximum density, at which the vehicles are nearly “bumper-to-bumper”—thus  $\ell = \rho_M^{-1}$  is the “effective” (uniform) vehicle length. Note that  $\ell$  is larger, by perhaps 25%–50%, than the actual length of a vehicle since true bumper-to-bumper conditions are not anticipated even in very dense traffic, and (ii)  $\tilde{u}_0$  is the drivers’ desired speed of travel on an otherwise empty road.

In this paper, we restrict ourselves to the representative form  $\tilde{u} = \tilde{u}_0(1 - \rho/\rho_M)^n$ , where  $n$  is “close” to 1. We defer the detailed treatment of the exact conditions on  $\tilde{u}$  that guarantee the existence of self-sustained nonlinear traveling waves in traffic to a later publication.

Ubiquitous attributes of the solutions to continuum traffic models are stable shocklike features, which may arise even in the absence of lane closures, traffic accidents, or other bottlenecks (see, e.g., Kerner and Konhäuser [8] and Aw and Rascle [10]). In analyzing such structures, a dissipative term proportional to  $u_{xx}$ , analogous to the viscous term in the Navier-Stokes equations, is often added to the right-hand side of the momentum Eq. (1.2) in order to “smear out” discontinuities [1]. However, the physical rationale for this term is ambiguous and the proper functional form is subject to debate. Solutions such as those obtained by Kerner and Konhäuser [8] and Kurtze and Hong [15], whose dynamics are nontrivially influenced by viscous dissipation, must therefore be interpreted with care. Herein, an alternative line

of inquiry is proposed: we seek self-sustained traveling wave solutions to the “inviscid” Eqs. (1.1) and (1.2) on a periodic or infinite domain, where shocks are modeled by discontinuities, as in the standard theory of shocks for hyperbolic conservation laws [16]. As we demonstrate below, not only do such nonlinear traveling waves exist, but they have a structure similar to that of the self-sustained detonation waves in the Zel’dovich-von Neumann-Doering (ZND) theory [17]. According to the ZND description, detonation waves represent shock waves with an attached exothermic reaction zone. In a self-sustained detonation wave, the flow downstream of the shock is subsonic relative to the shock, but accelerating to become sonic at some distance away from the shock. Hence, the flow behind a self-sustained detonation wave can be “transonic,” i.e., it may undergo a transition from subsonic to supersonic. The existence of the sonic point, the location where the flow speed relative to the shock equals the local sound speed, is the key feature in the ZND theory that allows one to solve for the speed and structure of the detonation wave. Its existence also means that the shock wave cannot be influenced by smooth disturbances from the flow further downstream so that the shock wave becomes self-sustained and independent of external forcing mechanisms. Hence the sonic point is an “acoustic” information or event horizon [18].

For the nonlinear traffic waves to be discussed herein, this means that their formation, due to small initial perturbations, is analogous to the ignition and detonation that can occur in a metastable explosive medium. Although this analogy has not, to our knowledge, been reported in the traffic literature, the physical and mathematical similarities between detonation waves and hydraulic jumps, described by equations similar to Eqs. (1.1) and (1.2), were recently pointed out by Kasimov [19]. (The analogy between hydraulic jumps and inert gas-dynamic shocks was recognized much earlier—see, e.g., Gilmore *et al.* [20] and Stoker [21].) As with Kasimov’s analysis, our aim is to herein exploit such commonalities to gain additional understanding into the dynamics of traffic flows, in particular, the traffic jams that appear in the absence of bottlenecks and for no apparent reason [14]. From this vantage point, insights are discerned over and above those that can be realized from the solution of a Riemann problem [10] or from the linear stability analysis of uniform base states [8,15,11]. Indeed, when such linear instabilities are present initially, our extensive numerical experiments suggest that the resulting “phantom jams” (see Helbing [1] and the many references therein) will ultimately saturate as nonlinear traveling waves, which we herein term “jamitons” and formally define as follows: In an inviscid macroscopic traffic model, a jamiton is the region of the nonlinear traveling wave between a shock and a sonic point, which travels unchanged at a constant velocity. The above observation provides a critical link between the initial and final states, the latter of which can, under select conditions (see, e.g., Sec. VD and Appendix A), be described analytically. Note as well that the above definition provides an important point of difference with the Korteweg–de Vries (KdV)-type traveling wave solutions described by Kurtze and Hong [15], Komatsu and Sasa [22] and others, which are obtained from a perturbation expansion in the long wavelength limit about a point

of linear instability. As we shall argue below, the present model, subject as it is to a different set of well-articulated assumptions, yields traveling waves of a different character, which apply over a broader expanse of traffic densities.

In the spirit of gas dynamics (and shallow water flows, astrophysics, etc.), shocks are introduced into the present (inviscid) model equations not because they serve as a literal description of particle dynamics in the vicinity of sharp gradients but rather as a mathematical idealization that allows otherwise inaccessible insights (e.g., the exact solutions discussed below) to be discerned [6,10]. The disadvantage of this approach is clear: we sacrifice any hope of accurately modeling traffic behavior in the vicinity of sharp gradients of density or speed. This is not to say, however, that our model equations make nonsensical predictions away from this shock transition region, which is, in all likelihood, not properly modeled even by a viscous (i.e., shock-free) continuum model. Indeed, as we illustrate by way of a detailed example in Sec. V, the exact solution offered by the inviscid equations gives a reasonable leading-order estimate for the shape of traveling wave solutions predicted by existing second-order traffic models over a range of traffic “viscosities.”

The rest of the paper is organized as follows: in Sec. II, we outline the basic requirements for Eqs. (1.1) and (1.2) to exhibit traveling wave solutions. To demonstrate the generality of this analysis, we consider in Sec. III modified forms for the momentum equation (developed by Aw and Rascle [10] and Helbing [11]). From this different starting point, the salient details of Sec. II shall be reproduced. The analysis is further generalized in Sec. IV, which considers a phase plane investigation of the governing equations from Secs. II and III. A particular example is studied, both theoretically and numerically, in Sec. V in which  $\tilde{u}$  and  $p$  are assigned particular functional forms. Conclusions are drawn in Sec. VI.

## II. TRAVELING WAVE SOLUTIONS

To determine periodic traveling wave solutions to the traffic flow Eqs. (1.1) and (1.2), we begin by making the solution ansatz,  $\rho = \rho(\eta)$  and  $u = u(\eta)$ , where the self-similar variable  $\eta$  is defined by

$$\eta = \frac{x - st}{\tau}. \quad (2.1)$$

Here  $s$  is the speed, either positive or negative, of the traveling wave. Equation (1.1) then reduces to

$$\{\rho(u - s)\}_{\eta} = 0, \quad \Rightarrow \rho = \frac{m}{u - s}, \quad (2.2)$$

where the constant  $m$  denotes the mass flux of vehicles in the wave frame of reference. Substituting Eq. (2.2) into Eq. (1.2), we obtain

$$\frac{du}{d\eta} = \frac{(u - s)(\tilde{u} - u)}{(u - s)^2 - c^2}, \quad (2.3)$$

where we interpret  $\tilde{u} = \tilde{u}(p)$  as a function of  $u$  via Eq. (2.2). Here  $c = (p_\rho)^{1/2} > 0$  is the “sound speed,” i.e., the speed at

which infinitesimal perturbations move relative to the traffic flow.

Equation (2.3) is a first-order ordinary differential equation and therefore, barring pathological and unphysical choices for  $c$  and  $\tilde{u}$ , does not admit any smooth periodic solutions. Hence, periodic traveling wave(s)—if they exist—must consist of monotone solutions to Eq. (2.3) that are connected by shocks. The simplest situation, as reproduced on a closed track in the experiment of Sugiyama *et al.* [14], is one in which there is exactly one shock (with speed  $s$ ) per period. The case of multiple shocks on a periodic or infinite road is somewhat more nuanced and shall receive a less detailed treatment here.

Before elaborating upon the solution attributes, we recall that shocks arising from differential equations of form (1.1) and (1.2) must satisfy two sets of conditions to be admissible. First, they must satisfy the Rankine-Hugoniot conditions [10,12,13], which follow from the conservation of mass and momentum, and ensure that shocks do not become sources or sinks of mass and/or momentum. Here, the Rankine-Hugoniot conditions read

$$s[\rho] = [\rho u] \quad (\text{i.e., conservation of mass}), \quad (2.4)$$

$$s[\rho u] = [p + \rho u^2] \quad (\text{i.e., conservation of momentum}), \quad (2.5)$$

where  $s$  is the shock speed and the brackets  $[ \ ]$  indicate the jump in the enclosed variable across the shock discontinuity. These equations relate the upstream and downstream conditions at the shock. In particular, let the superscripts  $+$  and  $-$  denote the states immediately downstream (right) and upstream (left) of the shock, respectively. Then Eq. (2.4) is equivalent to

$$\rho^+(u^+ - s) = m = \rho^-(u^- - s), \quad (2.6)$$

where the constant  $m$  is the mass flux across the shock. Of course, for a shock embedded as the upstream boundary of a jamiton, this  $m$  is the same as the one in Eq. (2.2).

In the spirit of many previous studies such as Kerner and Konhäuser [8], Kerner *et al.* [23], and Aw and Rascle [10], Eq. (2.5) is selected so as to be mathematically consistent with the system of partial differential equations given by Eqs. (1.1) and (1.2). In actuality, the extent to which momentum is conserved through regions of sharp traffic density variation is highly questionable. While deriving, from first principles, a more satisfactory shock conservation equation remains an open research topic, we emphasize that the solution algorithm to be discussed below is essentially independent of the form of the latter shock conservation equation. Thus, alteration of Eq. (2.5) would require but trivial modifications to the solution procedure.

The second set of conditions to be satisfied by the shock are the Lax “entropy” conditions [13,16], which enforce dynamical stability. In the case of shocks in gas dynamics, these conditions are equivalent to the statement that the entropy of a fluid parcel increases as it goes through the shock transition—hence the name. However, the existence of a physical entropy is not necessary for their formulation: sta-

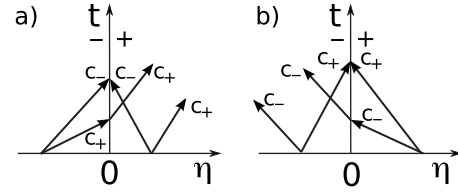


FIG. 1. Characteristics on both sides of a left (a) and right (b) shock in the frame of the shock. The flow direction is from left to right in (a) and right to left in (b). The equations of the characteristics are  $C_{\pm}: d\eta/dt = (u - s \pm c)/\tau$ , where  $\eta$  is defined by Eq. (2.1), and  $s$  is the shock speed.

bility considerations alone suffice. Furthermore, these conditions also guarantee that the shock evolution is causal.

For the particular system of equations in Eqs. (1.1) and (1.2), the Lax entropy conditions—given below in Eqs. (2.7) and (2.8)—state that one family of characteristics<sup>1</sup> must converge into the shock path in space time, while the other family must pass through it. Thus exactly two families of shocks are possible, as illustrated in Fig. 1: the left (respectively right) shocks have the left (respectively right) characteristics converging upon them.

The above discussion implies that two cases are possible, at least in principle: jamitons containing a left shock wherein the mass flux,  $m$ , is positive, see item 1 below, and jamitons containing a right shock wherein the mass flux,  $m$ , is negative; see item 2 below. However, as we argue after item 2, only jamitons with  $m > 0$  are mathematically consistent; self-sustained traveling waves carrying within them a right shock are not permitted. This agrees with the experiment of Sugiyama *et al.* [14] and with one’s everyday driving experience: it is situations where individual vehicles overtake shocks (hence  $m > 0$ ) that are observed in reality, rather than the converse.

Thus whereas in second-order traffic models information in the form of shock waves can travel downstream faster than individual vehicles [24], the results in this paper show that this cannot happen in the form of a self-sustained traveling wave. Further to the analysis of Aw and Rascle [10] and Helbing [11], this observation lends additional support to the conclusion that second-order models are not *ipso facto* flawed—see also Helbing [1], Sec. IIID7 and the references therein.

Let us now consider in some detail the two scenarios that can, at least in theory, arise. For simplicity, we study traveling waves with a single shock per period on a closed road; however, the ideas presented below can easily be extended to other configurations.

(1) The shock is the left shock, as in Fig. 1(a), so that

$$(u - c)^- > s > (u - c)^+. \quad (2.7)$$

In this case the mass flux must be positive, since  $m = \rho^-(u^- - s) > \rho^- c^- > 0$ . Moreover,  $\rho^+/\rho^- = (u - s)^-/(u - s)^+ > c^-/c^+$ , so

<sup>1</sup>The curves in space time along which infinitesimal perturbations propagate. Namely  $dx/dt = u + c$  (“right” characteristics) and  $dx/dt = u - c$  (“left” characteristics).

that  $\rho^+c^+ > \rho^-c^-$ . The traffic pressure  $p$  is a convex function of  $v = \rho^{-1}$  (see Sec. I), hence  $\rho c = (-dp/dv)^{1/2}$  is an increasing function of the traffic density. Thus  $\rho^+c^+ > \rho^-c^-$  implies that  $\rho^+ > \rho^-$ . In other words, the shock is compressive: the traffic density increases as the vehicles pass through the shock, traveling from left to right. Conversely, since  $u = s + m/\rho$ , it follows that  $u^- > u^+$  and, consequently, vehicles decelerate as they overtake the shock. It should then be clear that these shocks have all the familiar properties of traffic jams.

We conclude that for a traveling wave with a left shock, the continuous solution of Eqs. (2.1)–(2.3) must have a decreasing density,  $d\rho/d\eta < 0$ , and an increasing velocity,  $du/d\eta > 0$ . This follows because the solution must be a monotone function of  $\eta$  and must connect the postshock state  $(\rho^+, u^+)$  in one shock, to the preshock state  $(\rho^-, u^-)$  in the subsequent shock across a period in  $\eta$ —say from  $\eta=0$  to  $\eta=\lambda$ .

(2) The shock is the right shock, as in Fig. 1(b), so that

$$(u+c)^- > s > (u+c)^+. \quad (2.8)$$

The mass flux now is negative, since  $m = \rho^+(u-s)^+ < -\rho^+c^+ < 0$ . As in item 1, it is straightforward to show that  $u^- > u^+$  and  $\rho^- > \rho^+$ . For a traveling wave with a right shock, the continuous and monotone solution of Eqs. (2.1)–(2.3) must have both the density and velocity increasing with  $\eta$  (i.e.,  $d\rho/d\eta > 0$  and  $du/d\eta > 0$ ), in order to connect  $(\rho^+, u^+)$  to  $(\rho^-, u^-)$  across a period in  $\eta$ . Notice that the shock is again compressive: the traffic density (in the vehicles' frame of reference) increases as vehicles pass through the shock. However, in this latter case, the shock overtakes the vehicles from behind, which accelerate as they pass through the shock transition. This is a clearly counterintuitive situation, not observed in real traffic [24].

Fortunately, as we demonstrate next, traveling wave solutions with  $m < 0$  are mathematically inconsistent, which obviates the need to consider them any further. First, Eq. (2.2) is employed to rewrite Eq. (2.3) in the form

$$\frac{du}{d\eta} = m\rho G(\rho, s, m), \quad (2.9)$$

where

$$G = \frac{\tilde{u} - u}{m^2 - \rho^2 c^2}, \quad (2.10)$$

$m^2 - \rho^2 c^2 = \rho^2 \{(u-s)^2 - c^2\}$ , and  $u = s + m/\rho$ . Because  $du/d\eta > 0$ , a smooth solution connecting  $(\rho^+, u^+)$  to  $(\rho^-, u^-)$  requires  $G < 0$ . However,  $m^2 - \rho^2 c^2 = \rho(u-s+c)(m-\rho c)$  and  $m - \rho c < 0$ , and it follows from Eq. (2.8) that  $(m^2 - \rho^2 c^2)^+ > 0 > (m^2 - \rho^2 c^2)^-$ . Thus  $G < 0$  requires  $(\tilde{u} - u)^+ < 0 < (\tilde{u} - u)^-$ , which is impossible since  $\tilde{u}(\rho) - u = \tilde{u}(\rho) - s - m/\rho$  is a strictly decreasing function of  $\rho$ :  $\tilde{u}(\rho)$  decreases with increasing  $\rho$  by assumption and  $m < 0$ .

The difficulties documented in the previous paragraph are avoided for traveling waves with  $m > 0$ . In this case, we demand a solution of Eq. (2.9) with  $du/d\eta > 0$  and  $d\rho/d\eta < 0$ , connecting  $(\rho^+, u^+)$  to  $(\rho^-, u^-)$ . This in turn requires  $G > 0$  for  $\rho^- < \rho < \rho^+$ . The assumptions on  $p = p(\rho)$  imply that  $m^2 - \rho^2 c^2$  is a strictly decreasing function of  $\rho$  (item 1). Since

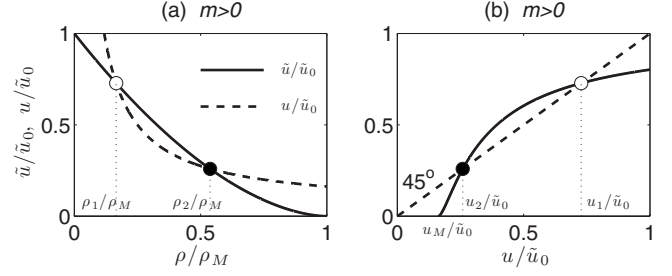


FIG. 2. (a) Typical profiles for  $\tilde{u}/\tilde{u}_0$  (solid curve) and  $u/\tilde{u}_0$  (dashed curve) as functions of  $\rho/\rho_M$ , where  $u = s + m/\rho$ . Equivalently, these profiles may be plotted against  $u/\tilde{u}_0$  by employing transformation (2.2), as shown in (b)—the dashed curve is then just a line with unit slope. The two curves will either not intersect at all, be tangent at a single point, or have two transversal intersections. The case of interest to us is the one with two transversal intersections, as depicted here:  $u_2$  is the intersection with a smaller velocity and a larger density  $\rho_2 = m/(u_2 - s)$ —solid circles, while the other intersection (open circles) defines  $u_1$  and  $\rho_1$ . In order to satisfy the conditions in Eq. (2.11), the sonic point must coincide with  $(u_2, \rho_2)$ . Finally, a physically meaningful solution requires  $u > 0$  everywhere. Hence,  $u_2 > 0$  is needed. As shown by panel (b), this condition is equivalent to the statement: when  $\tilde{u} = 0$ , that is  $\rho = \rho_M$ , the corresponding  $u = u_M = s + m/\rho_M$  is positive.

$m^2 - \rho^2 c^2 = \rho(u-s-c)(m+\rho c)$  with  $m+\rho c > 0$ , it follows from Eq. (2.7) that  $(m^2 - \rho^2 c^2)^- > 0 > (m^2 - \rho^2 c^2)^+$ . We conclude therefore that  $m^2 - \rho^2 c^2$  has a unique, multiplicity one, zero at some  $\rho_s$ , with  $\rho^- < \rho_s < \rho^+$ . In order for Eq. (2.9) to have a smooth solution with the desired properties, the numerator  $\tilde{u} - u = \tilde{u}(\rho) - s - m/\rho$  must be such that

$$\left. \begin{array}{l} \text{(a) } \tilde{u} - u \text{ has a simple zero at } \rho = \rho_s, \\ \text{(b) } \tilde{u} - u > 0 \text{ for } \rho^- \leq \rho < \rho_s, \\ \text{(c) } \tilde{u} - u < 0 \text{ for } \rho_s < \rho \leq \rho^+. \end{array} \right\} \quad (2.11)$$

This then guarantees not only that the zero in the denominator of Eqs. (2.9) and (2.10) is cancelled by a zero of the same order in the numerator, but that the resulting regularized ordinary differential equation yields  $du/d\eta > 0$  everywhere, as needed. Indeed,  $\rho_s$  is the traffic density at the sonic point, with corresponding flow speed  $u_s = s + m/\rho_s$ .

Figure 2 illustrates the situation, with plots of  $u$  and  $\tilde{u}$  as functions of  $\rho$  and  $u$  for representative initial conditions  $\rho^+$  and  $u^+$ . The shock speed,  $s$ , is here restricted by the inequalities  $u^+ > s > (u-c)^+$ . Clearly, the conditions in Eq. (2.11) require that the sonic point values of the density,  $\rho_s$ , and velocity,  $u_s$ , coincide with  $\rho_2$  and  $u_2$ . The sonic condition therefore reads

$$u_2 = s + c(\rho_2), \quad (2.12)$$

from which the jamiton speed,  $s$ , can be determined. With  $\rho_2$  and  $u_2$  defined as functions of  $(\rho^+, u^+, s)$  via Fig. 2, Eq. (2.12) is an algebraic equation that determines  $s$  as a function of  $(\rho^+, u^+)$ . In general, Eq. (2.12) must be solved numerically. Finally, we point out that (i) the restriction  $u_M > 0$  must be imposed, where  $u_M = s + m/\rho_M$  is the speed corresponding to the maximum traffic density  $\rho_M$ ; (ii) the cases of  $u_2 = u_1$ , where  $u_1$  is defined in Fig. 2, or of no intersections between

the solid and dashed curves of Fig. 2 do not yield jamitons.

The methodology summarized above is reminiscent of the related analyses in gas dynamics [17,18], shallow water theory [19,25,26], astrophysical accretion flow [27], and Newtonian flow in elastic tubes [28], where ordinary differential equations similar to Eq. (2.3) are obtained. Indeed, Eq. (2.12) is the exact analog of the Chapman-Jouguet condition in detonation theory [17].

Summarizing the above discussion, the following algorithm may be applied to determine the structure of a steady, nonlinear traveling wave on a closed, periodic roadway:

(i) For a prescribed downstream state,  $(\rho^+, u^+)$ , the regularization condition (2.12) specifies the permissible value(s) for the wave speed  $s$ .

(ii) Once  $s$  is determined, the state upstream of the shock,  $(\rho^-, u^-)$ , is computed using the Rankine-Hugoniot conditions (2.4) and (2.5).

(iii) Equation (2.3) is then integrated in  $\eta$ , from the initial condition  $u = u^+$  up until  $u = u^-$  is reached—the traffic density  $\rho$  follows automatically from Eq. (2.2). This defines the period  $\lambda$  of the traveling wave or, equivalently, the roadway circumference.

(iv) The total number of vehicles,  $\mathcal{N}$ , which remains fixed in time when there are no on-ramps or off-ramps, is then evaluated from

$$\mathcal{N} = \int_0^\lambda \rho dx. \quad (2.13)$$

On an open (i.e., infinite) roadway, smooth solutions are obtained by choosing  $(\rho^+, u^+)$  not so that  $\lambda$  takes on a particular value, but rather such that  $u_1 = u^-$ . For an isolated traveling wave, traffic conditions upstream and far downstream are therefore identical. The number of vehicles along an infinite roadway is unbounded and therefore Eq. (2.13) is not applicable. Even so, by suitable manipulation of Eq. (2.13), one can determine, for example, the number of vehicles between the shock and the sonic point.

The above algorithm provides a parametrization of the traveling waves using  $(\rho^+, u^+)$ . Equivalent parametrizations, in terms of  $(\rho^-, u^-)$ , are just as easy to produce. However, these are not necessarily ideal parametrizations. For example, in order to predict what traveling wave configuration might arise from a given set of initial conditions, on a given closed roadway,<sup>2</sup> a parametrization in terms of the roadway length,  $\lambda$ , and the total number of vehicles,  $\mathcal{N}$ , would be more desirable. On the other hand, for the example considered in Sec. V, and all the other case studies that we have examined to date,  $\rho^-$  maps in a one-to-one fashion to  $\mathcal{N}$ . Thus, by applying the above algorithm, one can iteratively determine the unique traveling wave solution corresponding to particular choices for the functions  $p$  and  $\tilde{u}$ , the parameters  $\tau$  and  $\lambda$ , and the average traffic density  $\rho_{avg} = \mathcal{N}\lambda^{-1}$ .

### III. ALTERNATIVE DESCRIPTION OF THE MOMENTUM EQUATION

The existence of self-sustained shock solutions is not specific to the details of the continuum model used. It is, in fact,

<sup>2</sup>Say to predict the patterns arising in the experiments by Sugiyama *et al.* [14].

a feature of models involving hyperbolic conservation laws with forcing terms under rather generic conditions. To illustrate this point, we shall briefly consider the equations presented by Aw and Rascle [10] and Helbing [11]. As an aside, these models were developed in response to the criticisms of Daganzo [24], who argued that second-order models are necessarily flawed—they predict, for example, shocks overtaking individual vehicles in unsteady traffic flow and negative vehicle speeds at the end of a stopped queue. Daganzo’s former criticism *ipso facto* does not apply to gas-kinetic macroscopic models where the traffic pressure is defined as the product of traffic density and velocity variance (i.e.,  $p = \rho\theta$ ), in which case shocks cannot overtake the fastest vehicles ([29]; see also [11]). Also, it was shown by Treiber *et al.* [29] that one can avoid the problem of negative vehicle speeds by replacing the viscous term, proportional, say, to  $u_{xx}$ , with a nonlocal interaction parameter, which offers comparable smoothing behavior but does not modify the hyperbolic nature of the underlying partial differential equation.

Returning to fully macroscopic models, Aw and Rascle [10] apply a convective, rather than a spatial, derivative when modeling the effects of preventive driving (the anticipation term in their nomenclature). This leads to the momentum Eq. (1.2) being replaced by

$$(u + p)_t + u(u + p)_x = \frac{1}{\tau}(\tilde{u} - u). \quad (3.1)$$

By substitution of the mass continuity equation (1.1), Eq. (3.1) can be rewritten as

$$u_t + (u - c^2\rho)u_x = \frac{1}{\tau}(\tilde{u} - u). \quad (3.2)$$

Introducing the self-similar variable  $\eta$  defined by Eq. (2.1), it can be shown that

$$\frac{du}{d\eta} = \frac{(u - s)(\tilde{u} - u)}{(u - s)^2 - mc^2}, \quad (3.3)$$

which is identical to Eq. (2.3), except that the sonic point is now predicted to occur when  $u - s = m^{1/2}c$ . As before, the singularity of Eq. (3.3)—i.e., the sonic point, where the denominator vanishes—is regularized by aligning the sonic point with a root of  $\tilde{u} - u$ . The remainder of the analysis is entirely similar to that outlined previously for Eqs. (1.1) and (1.2), with appropriate modifications to the shock conditions. Under the Aw and Rascle formulation, the Rankine-Hugoniot condition corresponding to the conservation of momentum takes the form

$$s[\rho(u + p)] = [\rho up + \rho u^2], \quad (3.4)$$

which replaces Eq. (2.5).

Helbing [11] generalized Aw and Rascle’s model one step further by defining two traffic pressures, both functions of  $\rho$  and  $u$ , such that the momentum equation reads

$$u_t + uu_x + \frac{1}{\rho} \frac{\partial p_1}{\partial \rho} \rho_x + \frac{1}{\rho} \frac{\partial p_2}{\partial u} u_x = \frac{1}{\tau}(\tilde{u} - u). \quad (3.5)$$

Proceeding as above, the following familiar expression can be readily obtained:

$$\frac{du}{d\eta} = \frac{(u-s)(\tilde{u}-u)}{(u-s)^2 - \varsigma^2}, \quad (3.6)$$

where

$$\varsigma^2 = c_1^2 + mc_2^2, \quad (3.7)$$

in which

$$c_1^2 = \frac{\partial p_1}{\partial \rho} \quad \text{and} \quad c_2^2 = -\frac{1}{\rho^2} \frac{\partial p_2}{\partial u}.$$

The Payne-Whitham and Aw and Rascle results may be recovered from Eq. (3.6) by setting, respectively,  $p_1=p$ ,  $p_2=0$ , and  $p_1=0$ ,  $p_2=-u\rho^2 dp/d\rho$ .

#### IV. PHASE PLANE ANALYSIS

Generalizing the discussion of Secs. II and III  $du/d\eta$  may be expressed as

$$\frac{du}{d\eta} = \frac{(u-s)(\tilde{u}-u)}{(u-s)^2 - \Omega c^2}, \quad (4.1)$$

where  $\Omega=1$  and  $m$ , respectively, for the Payne-Whitham and Aw and Rascle models. Further information regarding model behavior near the sonic point may be gleaned by introducing the phase plane variable  $\xi$ , and rewriting Eq. (4.1) as the following pair of ordinary differential equations:

$$\frac{du}{d\xi} = (u-s)(\tilde{u}-u) = F_1(u), \quad (4.2)$$

$$\frac{d\eta}{d\xi} = (u-s)^2 - \Omega c^2 = F_2(u). \quad (4.3)$$

Note that the sonic point is a critical point of Eqs. (4.2) and (4.3). The Jacobian,  $\mathcal{J}$ , of the above pair of equations is then given by

$$\mathcal{J} = \begin{bmatrix} F_{1,u} & 0 \\ F_{2,u} & 0 \end{bmatrix}, \quad (4.4)$$

where

$$F_{1,u} = -(u-s) \left\{ \frac{m\tilde{u}_\rho}{(u-s)^2} + 1 \right\} + \tilde{u} - u, \quad (4.5)$$

$$F_{2,u} = 2(u-s) + \frac{\Omega m}{(u-s)^2} p_{\rho\rho}, \quad (4.6)$$

in which

$$\tilde{u}_\rho \equiv \frac{d\tilde{u}}{d\rho} < 0 \quad \text{and} \quad p_{\rho\rho} \equiv \frac{d^2 p}{d\rho^2} = \frac{dc^2}{d\rho}.$$

Therefore, at the sonic point the eigenvalues ( $r_1$  and  $r_2$ ) of  $\mathcal{J}$  are given by

$$r_1 = 0 \quad \text{and} \quad r_2 = \frac{m|\tilde{u}_\rho|}{\Omega^{1/2}c} - \Omega^{1/2}c = F_{1,u}. \quad (4.7)$$

When  $r_2 > 0$  (respectively  $r_2 < 0$ ),  $du/d\eta > 0$  (respectively  $du/d\eta < 0$ ) at the sonic point. Because of the Lax entropy

conditions described earlier,  $u$  should be a monotonically increasing function of  $\eta$  away from a shock, which in turn requires

$$r_2 > 0 \Leftrightarrow m|\tilde{u}_\rho| > \Omega c^2. \quad (4.8)$$

Unfortunately, since  $r_1=0$ , the critical point is linearly degenerate. Thus a complete analysis of the solution behavior near this critical point requires a careful, but ultimately tangential, examination of the leading order contributions by nonlinearities. Nevertheless, an interesting observation can be made: as we illustrate by way of example in Sec. V  $r_2=0$  coincides with the boundaries wherein a constant uniform base state becomes unstable to infinitesimal disturbances.

The theoretical underpinnings of this coincidence are not entirely clear. However, our numerical experiments show that there is a strong connection between jamitons and instabilities: when a uniform traffic state is linearly unstable, the instability consistently saturates into a state dominated by nonlinear traveling waves.

For the more general analysis of Helbing [11] discussed at the end of Sec. III,  $F_{2,u}$  is given by

$$F_{2,u} = 2(u-s) + \frac{m}{(u-s)^2} \varsigma_\rho^2 = 2(u-s) + \frac{m}{(u-s)^2} p_{1,\rho\rho} + \frac{2(u-s)}{m} p_{2,u} - p_{2,u\rho}, \quad (4.9)$$

where  $\varsigma^2$  is defined by Eq. (3.7). Given the form of the Jacobian matrix  $\mathcal{J}$ , modifying  $F_{2,u}$  does not alter the eigenvalues  $r_1$  and  $r_2$ .

## V. EXAMPLE

### A. Preliminaries

To make the ideas of the previous sections more concrete, we consider herein particular forms for  $p$  and  $\tilde{u}$ , and carefully examine the resulting range of solutions. As alluded to above, various expressions for  $p$  and  $\tilde{u}$  have been proposed in the traffic literature. Consistent with the spirit of previous studies (e.g., [8,23]), our motivation is to select relatively simple functions so that the concepts of Sec. II are succinctly illustrated with a nonprohibitive algebraic investment. Thus, a Lighthill-Whitham-Richards forcing term of the form

$$\tilde{u} = \tilde{u}_0 \left( 1 - \frac{\rho}{\rho_M} \right) \quad (5.1)$$

is chosen. Moreover, we consider a traffic pressure of type

$$p = -\beta\{\rho + \rho_M \ln(\rho_M - \rho)\}, \quad (5.2)$$

so that  $p_\rho = c^2 = \beta\rho/(\rho_M - \rho)$ . With  $p$  so selected,  $\rho$  has as its strict upper bound the maximum traffic density,  $\rho_M$ .

Applying the above definitions to the Payne-Whitham model of Sec. I yields

$$\frac{du}{d\eta} = \frac{(\rho_M(u-s) - m)(u-s) \left\{ \tilde{u}_0 \left[ 1 - \frac{m}{\rho_M(u-s)} \right] - u \right\}}{\rho_M(u-s)^3 - m(u-s)^2 - \beta m}. \quad (5.3)$$

The denominator exhibits one real and two complex roots, the latter of which are assigned real and imaginary components  $a$  and  $b$ , respectively, i.e.,

$$\begin{aligned} & \rho_M(u-s)^3 - m(u-s)^2 - \beta m \\ &= \rho_M(u-s - U_c)(u-s - (a+ib))(u-s - (a-ib)). \end{aligned} \quad (5.4)$$

Here  $a$  and  $b$  can be calculated either analytically or numerically using a standard root solving algorithm. The sonic point is defined as

$$u-s = U_c \quad (5.5)$$

and the nontrivial zeros of the numerator are given by

$$\{u_1 - s, u_2 - s\} = \frac{1}{2}(\tilde{u}_0 - s) \pm \frac{1}{2}(\tilde{u}_0 - s) \left\{ 1 - \frac{4\tilde{u}_0 m}{\rho_M(\tilde{u}_0 - s)^2} \right\}^{1/2}. \quad (5.6)$$

The regularization condition (2.12) may therefore be written as

$$u_2 - s = U_c. \quad (5.7)$$

Upon canceling  $u-u_2$  from the numerator and denominator of Eq. (5.3), the resulting ordinary differential equation is integrable and yields as an implicit solution

$$\begin{aligned} \eta \{ \rho_M(u_1 - s) - m \} &= (u^+ - u) \{ \rho_M(u_1 - s) - m \} \\ &+ \rho_M \{ a^2 - 2a(u_1 - s) + b^2 \} \\ &+ (u_1 - s)^2 \ln \left\{ \frac{u_1 - u^+}{u_1 - u} \right\} + \left\{ \frac{m^2}{\rho_M} - 2am \right. \\ &+ (a^2 + b^2) \rho_M \left. \right\} \ln \left\{ \frac{\rho_M(u-s) - m}{\rho_M(u^+ - s) - m} \right\}. \end{aligned} \quad (5.8)$$

By definition on a periodic roadway,  $u = u^-$  when  $\eta\tau = \lambda$ , where  $\lambda$  is the roadway circumference. Therefore,  $\lambda$  can be determined from

$$\begin{aligned} \frac{\lambda}{\tau} \{ \rho_M(u_1 - s) - m \} &= (u^+ - u^-) \{ \rho_M(u_1 - s) - m \} \\ &+ \rho_M \{ a^2 - 2a(u_1 - s) + b^2 \} \\ &+ (u_1 - s)^2 \ln \left( \frac{u_1 - u^+}{u_1 - u^-} \right) + \left\{ \frac{m^2}{\rho_M} - 2am \right. \\ &+ (a^2 + b^2) \rho_M \left. \right\} \ln \left\{ \frac{\rho_M(u^- - s) - m}{\rho_M(u^+ - s) - m} \right\}. \end{aligned} \quad (5.9)$$

Starting from Eq. (2.13), the total number of vehicles along the periodic roadway can be computed from

$$\mathcal{N} = \int_0^\lambda \rho dx = \tau \int_0^{\eta_{\max}} \rho d\eta = m\tau \int_{u^+}^{u^-} \frac{1}{u-s} \left( \frac{du}{d\eta} \right)^{-1} du. \quad (5.10)$$

Application of Eq. (5.3) in Eq. (5.10) shows that

$$\begin{aligned} & \mathcal{N} \frac{(u_1 - s)}{\tau} \{ m - \rho_M(u_1 - s) \} \\ &= \{ m^2 - 2a\rho_M m + (a^2 + b^2)\rho_M^2 \} (u_1 - s) \\ &\quad \times \ln \left\{ \frac{\rho_M(u^+ - s) - m}{\rho_M(u^- - s) - m} \right\} + \rho_M m \{ a^2 - 2a(u_1 - s) \\ &\quad + b^2 + (u_1 - s)^2 \} \ln \left( \frac{u_1 - u^-}{u_1 - u^+} \right) + (a^2 + b^2) \\ &\quad \times \rho_M \{ \rho_M(u_1 - s) - m \} \ln \left( \frac{u^- - s}{u^+ - s} \right), \end{aligned} \quad (5.11)$$

from which  $\mathcal{N}$  can easily be obtained. As noted earlier,  $\mathcal{N}$  is unbounded on an infinite roadway.

Comparable exact solutions may also be determined for the popular simpler cases  $p \propto \rho^\gamma$  with  $\gamma = 1, 2$  [9,10,23]. These are presented in Appendix A.

## B. Linear stability

In Appendix B we compute the boundaries between linearly stable and unstable uniform base states, which are given by

$$\frac{\rho}{\rho_M} = \frac{1}{2} \left\{ 1 \pm \left( 1 - \frac{4\beta}{\tilde{u}_0^2} \right)^{1/2} \right\}. \quad (5.12)$$

According to this result, instabilities generally disappear in either very light traffic where driver interactions are minimal or in very congested traffic where there is limited opportunity for establishing alternating bands of heavy and moderate traffic, such is the magnitude of the background traffic density (cf. Fig. 6 of Treiber *et al.* [29]).

The stability bounds specified by Eq. (5.12) apply to both open and closed roadways and indicate the locations at which either  $u_2 = 0$  (plus sign) or  $u_1 = u_2$  (minus sign), where  $u_1$  and  $u_2$  are defined in Fig. 2. Once  $u_1$  and  $u_2$  coalesce, no self-sustained shock wave may occur—since condition (a) in Eq. (2.11) fails. Thus jamitons become possible when the corresponding uniform state becomes unstable and the basic flow state changes from uniform flow to a (nonlinear) wave-dominated state. In other words, evidence indicates that a crucial bifurcation in the traffic flow behavior occurs at the stability boundaries prescribed by Eq. (5.12). We defer a more in-depth investigation of this question for future work. Note that although the lower boundary specified by Eq. (5.12) is mathematically robust, in practice it may become “fuzzy” owing to the possible breakdown of the continuum hypothesis at low vehicle concentrations.

## C. Numerical method

In order to validate the aforementioned theoretical solutions and assess traveling wave stability, we performed nu-

merical simulations using a Lagrangian particle method [30]. In this method, each discrete particle,  $i$ , is assigned an initial position,  $x_i$ , and speed,  $u_i$ , which subsequently changes in time according to Eqs. (5.13)–(5.18). The mass balance Eq. (1.1) is satisfied identically as the particles move, i.e., the numerical scheme is mass conservative by construction. Importantly, the number of particles is typically 2 orders of magnitude larger than the number of vehicles. Thus, although a Lagrangian approach is employed, the numerical scheme constitutes a macroscopic, not a microscopic, description of traffic flow, albeit one with an intuitive link between the particle and vehicle density.

In general terms, the numerical method solves the differential equations

$$\begin{cases} \dot{x}_i = u_i, \\ \dot{u}_i = a_i, \end{cases} \quad (5.13)$$

where the particle acceleration,  $\dot{u}_i$ , is expressed as

$$\frac{du}{dt}(x_i, t) = u_i(x_i, t) + uu_x(x_i, t), \quad (5.14)$$

and

$$\begin{aligned} a_i = & -\frac{c(\rho(x_i, t))^2}{\rho(x_i, t)} \rho_x(x_i, t) + \frac{1}{\tau} \{ \tilde{u}(\rho(x_i, t)) - u(x_i, t) \} \\ & + \frac{\mu}{\rho(x_i, t)} u_{xx}(x_i, t). \end{aligned} \quad (5.15)$$

Consistent with the related studies of Kerner and Konhäuser [8,9] and Kerner *et al.* [23], an explicit viscous damping term, with a diffusion coefficient  $\mu/\rho$ , is included on the right-hand side of Eq. (5.15). A distinction is drawn between two classes of numerical simulations: those for which (i) the  $u_{xx}$  term is included solely for numerical stabilization purposes, i.e., viscosity is included in the flavor of Lax and Wendroff [31] and is of comparable order to the numerical viscosity, which diminishes as the resolution is increased, and, (ii) the magnitude of the viscous term is comparable to that of the anticipation and relaxation terms, mimicking the numerical solutions previously obtained by Kerner and collaborators. When  $\mu$  is set identically to zero, the numerical solution is characterized by spurious oscillations immediately downstream of the shock.

The distance between adjacent particles  $i$  and  $i+1$  is defined by  $d_{i+1/2} = x_{i+1} - x_i$ . Then the interparticle density is computed by

$$\rho_{i+1/2} = \frac{\vartheta}{d_{i+1/2}}, \quad (5.16)$$

where  $\vartheta = \mathcal{N}/N_p$ —in which  $\mathcal{N}$  is the number of vehicles [as specified by Eq. (2.13)] and  $N_p$  is the number of particles. From Eq. (5.16), we define the vehicle density and the density gradient using a nonequidistant finite-difference stencil [32]:

$$\rho_i = \frac{d_{i+1/2}\rho_{i-1/2} + d_{i-1/2}\rho_{i+1/2}}{d_{i+1/2} + d_{i-1/2}}, \quad (5.17)$$

$$\rho_{i,x} = \frac{\rho_{i+1/2} - \rho_{i-1/2}}{\min\{d_{i+1/2}, 2d_{i-1/2}\} + \min\{d_{i-1/2}, 2d_{i+1/2}\}}. \quad (5.18)$$

The denominator in Eq. (5.18) is chosen so that, at the location of the shock, a given particle is influenced only by its nearest neighbor. The term proportional to  $u_{xx}$  from Eq. (5.15) is treated in a manner analogous to  $\rho_{i,x}$ .

## D. Results

### 1. Periodic roadway

Here we compare the theory of self-sustained traffic jams developed in Secs. II and V A with the numerical solutions of Eqs. (1.1) and (1.2)—obtained by applying the algorithm of Sec. V C with periodic boundary conditions. Employing the forcing and traffic pressure terms specified in Eqs. (5.1) and (5.2), the inviscid equations have the nondimensional form

$$\left. \begin{aligned} \rho_{t^*} + (u^* \rho^*)_{x^*} &= 0, \\ \Gamma_1(u_{t^*}^* + u^* u_{x^*}^*) + (\Gamma_2/\rho^*) \rho_{x^*}^* &= 1 - \rho^* - u^*, \end{aligned} \right\} \quad (5.19)$$

where  $\Gamma_1 = \tau \tilde{u}_0 \rho_M$ ,  $\Gamma_2 = \beta \tau \rho_M / \tilde{u}_0$ , and  $p^* = -\rho^* - \ln(1 - \rho^*)$ . The nondimensional and dimensional variables are related via

$$\rho = \rho_M \rho^*, \quad u = \tilde{u}_0 u^*, \quad x = \ell x^*, \quad \text{and} \quad t = (\ell/\tilde{u}_0) t^*. \quad (5.20)$$

The nondimensional traveling wave speed is defined by  $s^* = s/\tilde{u}_0$ .

As with the experiment of Sugiyama *et al.* [14], we consider a closed periodic track of length 230 m and select for the effective vehicle length  $\ell = 5$  m. The relaxation time scale is chosen as  $\tau = 2.5$  s whereas  $\beta = 4$  m<sup>2</sup>/s<sup>2</sup>. Finally,  $\tilde{u}_0 \approx 16.0$  m/s is selected such that, at the traffic density prescribed in the experiment of Sugiyama *et al.* [14], the desired speed of travel,  $\tilde{u}$ , is 8.33 m/s (30 km/h). With this choice of parameters,

$$\Gamma_1 \approx 8.0, \quad \Gamma_2 \approx 0.13. \quad (5.21)$$

Note that  $\beta = c^2(\rho_M/\rho - 1)$  is related to the speed at which disturbances propagate through traffic. Because a description, both theoretical and numerical, of jamitons is the central focus of the present analysis, we deliberately select a value for  $\beta$  toward the lower end of its representative range, so as to facilitate an explicit display of nonlinear traveling wave properties and behavior. Hence,  $\beta$ , whose exact numerical value is likely difficult to estimate in any event, is chosen so that infinitesimal perturbations to a uniform base state develop into nonlinear traveling waves when the base-state density is a small fraction of  $\rho_M$ —see Appendix B and, more particularly, the stability condition (5.12). Whereas larger numerical values for  $\beta$  could be considered, corresponding to a more restrictive instability condition, the jamitons observed in these cases, though qualitatively equivalent to those described below, are somewhat less easy to visualize. The practical ramifications associated with choosing a larger value for  $\beta$  are briefly addressed following our discussion of Fig. 4.

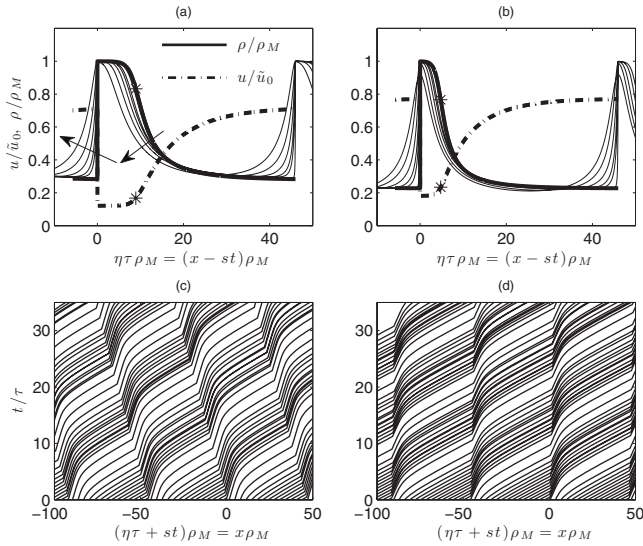


FIG. 3. [(a) and (b)] Comparison of theoretical (thick curves) and numerical (thin curves) solutions. The numerical solutions are the final asymptotic state of an evolution started with a small perturbation of a uniform unstable base state. Numerical results are either nominally inviscid or are obtained selecting  $\Gamma_3 = 1.5, 2.5, 5.0, 10, 20$ , where  $\Gamma_3 \equiv \tau\rho_M\mu$ . Arrows show the direction of increasing traffic viscosity  $\mu$  [see Eq. (5.15)]. The panels show profiles of  $\rho/\rho_M$  and  $u/\bar{u}_0$  versus  $\eta\tau\rho_M = (x-st)\rho_M$ . In the latter case, numerical results are omitted for clarity. Equations and parameters are as in Eqs. (5.19)–(5.21), with  $\lambda=46\ell=230$  m. In (a),  $\mathcal{N}=22$  mimicking the experiment of Sugiyama *et al.* [14]. In (b),  $\mathcal{N}=16$ . Stars indicate the sonic point. Corresponding representative vehicle trajectories, reconstructed from the theoretical solution, are also shown in (c) and (d) where, in both cases, vehicles move from left to right.

The steady-state variations of  $u^*$  and  $\rho^*$ , as functions of the nondimensional variable  $\eta\tau\rho_M = x^* - s^*\tau$ , are shown in Fig. 3 for a circular road of length  $\lambda=46\ell=230$  m, with two different choices for the conserved number of vehicles,  $\mathcal{N}$ . The shock occurs at the two extreme ends of the horizontal domain and connects the ratios  $u^-/\bar{u}_0$  to  $u^+/\bar{u}_0$ , and  $\rho^-/\rho_M$  to  $\rho^+/\rho_M$ . For both Figs. 3(a) and 3(b), the maximum observed traffic density is very close to  $\rho_M$ . The desired speed of travel is in this circumstance effectively nil, however, the actual speed of travel remains finite, if rather small.

Both theoretical and numerical data are included in Fig. 3. The comparison between the theoretical and nominally inviscid numerical solutions is very favorable, except right at the shock location where we observe numerical smearing, which diminishes as the resolution is increased. As expected, with increasing traffic viscosity, it is observed from Figs. 3(a) and 3(b) that the waveform becomes more symmetric. For moderate traffic viscosities (i.e.,  $\Gamma_3 \equiv \tau\rho_M\mu \lesssim 5.0$ ), Eq. (5.9) gives a good leading order description of the traffic density profile.

In Fig. 3(a),  $\mathcal{N}=22$ ; as with Sugiyama *et al.*'s experiment, the inviscid solution predicts that  $s < 0$  whereby the jamiton moves upstream against the direction of traffic flow. This is illustrated by Fig. 3(c), in which representative vehicle trajectories, as determined from the theoretical solution, are exhibited. For the selected values of  $\tau$  and  $\beta$ , theory predicts

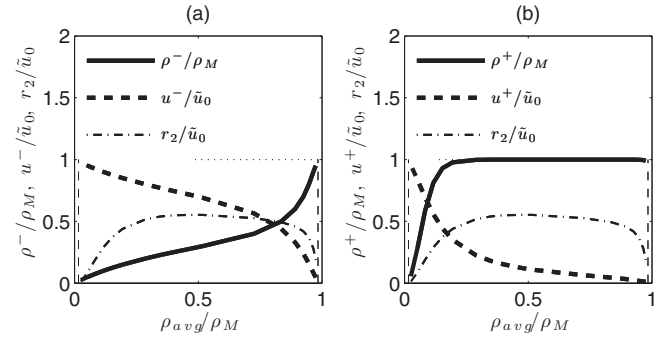


FIG. 4. Parameters characterizing the exact solutions in Sec. V A, for a fixed road length  $\lambda=46\ell=230$  m, as functions of the number of vehicles,  $\mathcal{N}$ , or, equivalently, the average nondimensional traffic density  $\rho_{avg}/\rho_M = \mathcal{N}/(\lambda\rho_M)$ . Specifically, curves of  $\rho^-/\rho_M$ ,  $\rho^+/\rho_M$ ,  $u^-/\bar{u}_0$ , and  $u^+/\bar{u}_0$  are shown, in addition to  $r_2/\bar{u}_0$  — as given in Eq. (4.7). The vertical dashed lines specify the linear stability boundaries  $\rho_{avg}/\rho_M=0.016$  and  $\rho_{avg}/\rho_M=0.984$  indicated by Eq. (5.12). The equations and parameters are as in Eqs. (5.19)–(5.21). Note that  $r_2$  goes through 0 precisely at the stability boundaries whereupon  $[\rho]=0$ ,  $[u]=0$ .

that  $s = -1.8$  m/s. This value is less (in absolute value) than, but of the same order as, the traveling wave speed of  $s \approx -5.6$  m/s measured by Sugiyama *et al.* [14]. The quantitative disagreement between theory and experiment is not wholly unexpected: as noted by Helbing [1], “...[the] Kerner-Konhäuser model is rather sensitive to the choice of parameters and the velocity-density relation.” In light of this comparison, we conclude that the canonical linear relationship proposed in Eq. (5.1), though analytically expedient, is probably too simple to capture the true richness of driving behavior. Better agreement between theory and experiment would most likely be obtained by choosing more complicated functional forms for the equilibrium speed [e.g.,  $\bar{u} = \bar{u}_0(1-\rho/\rho_M)^n$ ] and also the traffic pressure [e.g.,  $p_\rho = \beta\rho/(\rho_M-\rho)^q$ ]. However, these avenues of research are reserved for future investigations.

Contrasting the data of Figs. 3(a) and 3(c) ( $\mathcal{N}=22$ ) with that of Figs. 3(b) and 3(d) ( $\mathcal{N}=16$ , a circumstance not considered by Sugiyama *et al.* [14]) shows that the breadth of the downstream disturbance, formally defined as the jamiton width, i.e., the distance from the shock to the sonic point, decreases with the background traffic density,  $\rho_{avg} = \mathcal{N}/\lambda$ . Also, as indicated by Fig. 3(d),  $s > 0$  when  $\mathcal{N}=16$ , so that the jamiton moves with, not against, traffic.

Model sensitivity to the choice of parameters is manifest in a second, more subtle, fashion, namely in that  $s$  increases nontrivially with traffic viscosity  $\mu$  [see Eq. (5.15)]. Thus whereas  $s = -1.9$  m/s for the nominally inviscid numerical simulation with  $\mathcal{N}=22$  (in good agreement with the theoretical result reported above),  $s = -0.54$  m/s (respectively  $s = 1.8$  m/s) when  $\Gamma_3 = 5.0$  (respectively  $\Gamma_3 = 20$ ). Correspondingly with  $\mathcal{N}=16$ , it is observed that  $s = 0.30$  m/s, 2.4 m/s, and 5.2 m/s respectively, when the viscous damping is negligible and  $\Gamma_3 = 5.0, 20$ .

Figure 4 indicates, as a function of the normalized background traffic density  $\rho_{avg}/\rho_M$ , the range of possible solutions allowed by the model equations in Sec. V A on a closed

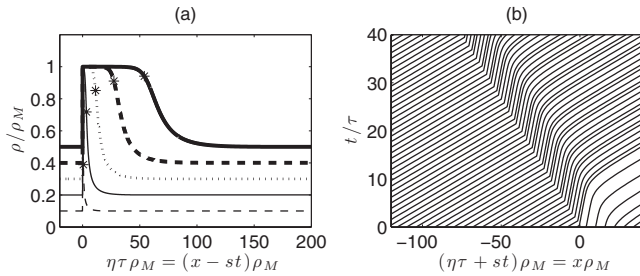


FIG. 5. (a) Theoretical profiles of the traffic density through a jamiton on an infinite road with various  $\rho_{\pm\infty}$ . As with Fig. 3, stars denote the sonic point. (b) Representative vehicle trajectories for  $\rho_{\pm\infty}/\rho_M=0.35$ .

roadway. For a prescribed road length  $\lambda$  and model parameters  $\rho_M$ ,  $\tilde{u}_0$ ,  $\beta$ , and  $\tau$ , the average density  $\rho_{avg}$  (hence  $\mathcal{N}$ ) uniquely determines the flow conditions to either side of the shock. The thick solid curves of Figs. 4(a) and 4(b) show  $\rho^-/\rho_M$  and  $\rho^+/\rho_M$ , respectively, whereas the thick dashed curves show  $u^-/\tilde{u}_0$  and  $u^+/\tilde{u}_0$ , respectively. Note that the jamiton amplitude becomes smaller as the corresponding uniform flow becomes less unstable, i.e.,  $[\rho]$  and  $[u]$  both disappear at the linear stability boundaries, which are given by the solution of Eq. (5.12) and are indicated in Fig. 4 by the thin vertical dashed lines. Consistent with the previous discussion,  $r_2$  also vanishes in these limits.

From Figs. 3(a), 3(b), and 4(b), we conclude that localized patches of high traffic density may arise even when the background traffic density is relatively low. In particular, the thick solid curve of Fig. 4(b) indicates that  $\rho^+ > 0.95\rho_M$  for  $\rho_{avg} < 0.2\rho_M$ . Needless to say, this simple result is not universal for all types of traffic flow or roadway conditions. We consider herein a periodic track of prescribed length (230 m), particular functional forms for the traffic pressure,  $p$ , and equilibrium speed,  $\tilde{u}$ , and a liberal numerical value for  $\beta$  such that steady nonlinear traveling waves appear even in relatively light traffic. Choosing a larger value for  $\beta$  would delay, though almost certainly not avoid, the onset of high density patches, which carry a high risk of vehicular collisions.

## 2. Infinite roadway

As indicated by the traffic density profiles of Fig. 5(a), qualitatively similar behavior is noted on open, as opposed to closed, roadways. In Fig. 5(a), the traffic density upstream and far downstream of the shock is given as  $\rho_{\pm\infty}/\rho_M = 0.1, 0.2, \dots, 0.5$ . Figure 5(b) shows representative vehicle trajectories for the case  $\rho_{\pm\infty}/\rho_M = 0.35$  and exhibits encouraging agreement with the measured observational data of Treiterer, which are reproduced in Fig. 6.

Consistent with related studies, a wrinkle that arises from the numerical study of traveling wave solutions on infinite and long periodic roadways is the appearance of multiple density peaks. In Sec. V D 1, and indeed in the experiment of Sugiyama *et al.* [14], the length of the periodic roadway was short enough so that a single (stable) nonlinear traveling wave arose from a perturbed, linearly unstable initial state. On an extended circuit, by contrast, the traveling wave solu-

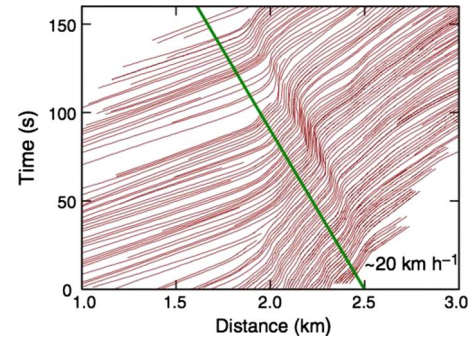


FIG. 6. (Color online) Measured vehicle trajectories due to Treiterer. The straight line shows the experimental measurement of Sugiyama *et al.* [14] (figure reproduced from Sugiyama *et al.* [14] with permission).

tions exhibit a long, nearly constant state downstream of the shock—whose average density exceeds the requirement for linear stability specified by Eq. (5.12). Thus, in the numerical simulations, infinitesimal perturbations may grow, leading to further traveling waves, albeit of slightly different amplitude from the original. These traveling waves are dynamically independent in that wave coalescence does not occur for a rather long time, if at all.

Traffic dynamics on a long (nonperiodic) road as resolved using the nominally inviscid numerical model of Sec. V C are illustrated in Fig. 7, which illustrates, in a manner reminiscent of the roll waves that appear in gutters on rainy days, the development of a train of jamitons [1]. From an initial disturbance, a sequence of nonlinear traveling waves is formed in succession; those at the upstream side of the wave train evolve most rapidly. Our (steady-state) theoretical solution provides an increasingly more accurate estimate of the density profile of an individual wave within the train as saturation is approached. Estimating the distance between successive jamiton crests is a mathematically laborious task [26,33] and shall not be pursued here.

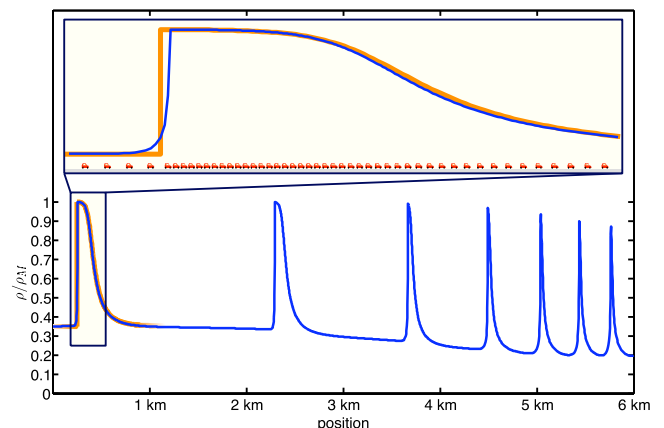


FIG. 7. (Color online) Multiple jamitons on a long (nonperiodic) road. Light and dark curves show, respectively, the theoretical and nominally inviscid numerical solutions. The difference is visible only in the expanded inset, which also presents a representative distribution of individual vehicles along the bottom. Here, for technical reasons, we select  $\Gamma_1=20$  and  $\Gamma_2=0.5$ . Qualitatively identical results are obtained with  $\Gamma_1 \approx 8.0$  and  $\Gamma_2 \approx 0.13$ .

## VI. CONCLUSIONS

In this work, we have found and successfully exploited a strong similarity between gas-dynamical detonation waves and shocks in traffic flow, in order to develop a theory of steady self-sustained traffic shocks. These features naturally arise from small instabilities in relatively dense traffic flow, and can be interpreted as saturated phantom jams. While a single nonlinear traveling wave may not necessarily significantly delay individual vehicles, a succession of waves, as might arise during rush hour, for example, is expected to frustrate motorists over long lengths of roadway (Fig. 7). Moreover, these waves represent regions in which the traffic density increases dramatically over a relatively short distance [14] and, as such, are hot spots for vehicular collisions.

The analogy drawn above goes beyond the weaker comparison with inert shock waves in gas dynamics considered by Kerner *et al.* [23]. Unlike inert shocks, detonation waves can be self-sustained due to the existence of a sonic point in direct correspondence with the traffic model we consider here. Even so, there exist important differences between jamitons (formally defined in Sec. I) and detonation waves, most especially in that the former may arise as a member of a train of nonlinear traveling waves. This behavior is not characteristic of detonation waves.

The appearance of a sonic point is significant for a second reason, namely, that the sonic point is an information boundary. As with the gas-dynamical example to which we make an extensive comparison, the flow is smooth near the sonic point and no dramatic change can be seen in the flow variables at that location. However, for the inviscid equations considered here, the sonic point precludes any influence from the downstream traffic on the jamiton structure. Thus no matter how quickly vehicles downstream of the sonic point escape the jam, the jamiton properties (in particular, the maximum traffic density), will not be affected. For real traffic flows, this suggests that one cannot easily relax the congested conditions that arise within a saturated phantom jam by modifying the traffic downstream of the sonic point. This observation helps to explain why phantom jams, once formed, may be difficult to dissipate.

Finally, because information in the form of smooth disturbances cannot cross the sonic point, one can replace, in a mathematical sense, the sonic point with a boundary where the boundary conditions are based on sonic condition (2.12). This has the potential of simplifying model validation and estimation with measured data since one may be able to analyze isolated segments of traffic without having to consider, for example, an entire freeway network. The simplification comes at a price, however: identification of sonic points from real data sets requires approximation of the traffic “sound speed”  $c$ , which may, in turn, require an estimate of the variation in the traffic pressure,  $p$ , with the traffic density,  $\rho$ , through a constitutive equation of the type given by Eq. (5.2). While the associated complications appear from a distance to be manageable (the constitutive equation is after all a component of the model that is being tested), we do not pursue this line of investigation in this preliminary study.

Critically, saturated phantom jams are of a qualitatively different character to the traffic jams that arise in the pres-

ence, rather than in the absence, of bottlenecks. For this more familiar class of blockages, the leading edge of the traffic density bulge is fixed in space at the position of the traffic accident, lane closure, etc. Meanwhile, the trailing edge propagates upstream. However, once the bottleneck is removed, uniform traffic flow is typically recovered, often rapidly so, i.e., “bottleneck jams” are not self-sustaining in the manner of saturated phantom jams. Accordingly, we shall defer an examination of the growth, saturation, and decay of bottleneck jams to a future publication (see also Helbing [1] and the many references therein). We point out in passing, however, that bottleneck jams may be more naturally analogous to overdriven, rather than Chapman-Jouguet, detonations (Fickett and Davis [17]).

Using the Lax entropy conditions for hyperbolic conservation laws, we show that for realistic pressure and equilibrium-speed functions, the only allowable self-sustained shocks are those that are overtaken by individual vehicles. Moreover, for the choices

$$\tilde{u} = \tilde{u}_0 \left( 1 - \frac{\rho}{\rho_M} \right), \quad p = \beta \{ \rho + \rho_M \ln(\rho_M - \rho) \}$$

(and also  $p \propto \rho^\gamma$ , with  $\gamma = 1, 2$ —see Appendix A), we are able to describe the nonlinear traveling wave structure analytically. Theoretical solutions show excellent agreement with the output from direct numerical simulations of the nominally inviscid governing equations.

Examples of nonlinear traveling waves on closed and open roadways are illustrated in Figs. 3 and 5, respectively. In the former case, and for the choice of parameters selected here, it is observed from Fig. 4 that the peak traffic density (i.e., the density just downstream of the traffic shock) often differs little from the maximum traffic density,  $\rho_M$ . Conversely, so as to minimize the likelihood of vehicular collisions, it is advantageous to select speed limits and roadway carrying capacities so as to avoid circumstances where traffic densities with  $\rho \simeq \rho_M$  are “triggered” (say, by a jamiton) anywhere within the domain.

Having identified self-sustained traveling wave solutions in traffic flow, major objectives of future research are to (i) ascertain the waves’ spatiotemporal stability [15], which is particularly important when studying traffic patterns on long (nonperiodic) roads (Fig. 7), and, (ii) establish, via rigorous first-principles arguments, the appropriate jump conditions to be applied at the traffic shock. In the present analysis, it is assumed, consistent with Kerner and Konhäuser [8], Kerner *et al.* [23] and Aw and Rascle [10], that both mass and momentum are conserved through regions of sharp density variation. Incorporating a suitable (i.e., non-*ad hoc*) momentum dissipation term is expected to alter some of the details from the examples considered in Sec. V, most notably by lowering the number of vehicles near the maximum traffic density. It must be reiterated, however, that the steps to be applied in deriving traveling wave solutions are insensitive to the choice of jump conditions so that the algorithm of Sec. II would remain essentially unchanged even if Eq. (2.5) were to be replaced by an alternate, and more appropriate, expression relating the momentum on the upstream and downstream sides of the traffic shock.

**ACKNOWLEDGMENTS**

Funding for M.R.F. was provided through the NSERC Discovery Grant Program. Funding for A.R.K. was provided through the USAFOSR Young Investigator Program under Grant No. FA9550-08-1-0035. Partial funding for J.-C.N., R.R.R., and B.S. was provided through NSF Grant No. DMS-0813648. We thank Dr. P. M. Reis for bringing to our attention the study of Sugiyama *et al.* [14].

**APPENDIX A: EXACT SOLUTIONS**  
WHEN  $p \propto \rho^\gamma$  with  $\gamma=1,2$

Equations (5.8), (5.9), and (5.11) specify, respectively, exact analytical solutions for  $u$ ,  $\lambda$  and  $\mathcal{N}$  when  $p$ , defined by Eq. (5.2), exhibits a logarithmic singularity in  $\rho$ . Correspond-

ing expressions, valid when  $p \propto \rho^\gamma$ , with  $\gamma=1,2$  are provided below.

(i)  $\gamma=1$ ,

$$\eta = u^+ - u + (u_1 - s + \beta^{1/2}) \ln \left( \frac{u_1 - u^+}{u_1 - u} \right), \quad (A1)$$

$$\frac{\lambda}{\tau} = u^+ - u^- + (u_1 - s + \beta^{1/2}) \ln \left( \frac{u_1 - u^+}{u_1 - u^-} \right), \quad (A2)$$

$$\mathcal{N} = m\tau \left\{ \frac{\beta}{u_1 - s} \ln \left( \frac{u^- - s}{u^+ - s} \right) + \left( 1 + \frac{\beta}{u_1 - s} \right) \ln \left( \frac{u_1 - u^+}{u_1 - u^-} \right) \right\}. \quad (A3)$$

(ii)  $\gamma=2$ ,

$$\eta = u^+ - u + \frac{(\beta m)^{2/3}}{u_1 - s} \ln \left( \frac{u - s}{u^+ - s} \right) + \left\{ (\beta m)^{1/3} + u_1 - s + \frac{(\beta m)^{2/3}}{u_1 - s} \right\} \ln \left( \frac{u_1 - u^+}{u_1 - u} \right), \quad (A4)$$

$$\frac{\lambda}{\tau} = u^+ - u^- + \frac{(\beta m)^{2/3}}{u_1 - s} \ln \left( \frac{u^- - s}{u^+ - s} \right) + \left\{ (\beta m)^{1/3} + u_1 - s + \frac{(\beta m)^{2/3}}{u_1 - s} \right\} \ln \left( \frac{u_1 - u^+}{u_1 - u^-} \right), \quad (A5)$$

$$\mathcal{N} = m\tau \left\{ \frac{(\beta m)^{2/3}}{u_1 - s} \left\{ \frac{u^- - u^+}{(u^- - s)(u^+ - s)} \right\} + \frac{(\beta m)^{1/3}}{u_1 - s} \left\{ \frac{(\beta m)^{1/3}}{u_1 - s} + 1 \right\} \ln \left\{ \frac{(u^- - s)(u_1 - u^+)}{(u^+ - s)(u_1 - u^-)} \right\} + \ln \left( \frac{u_1 - u^+}{u_1 - u^-} \right) \right\}. \quad (A6)$$

Equation (A4) bears a striking resemblance to Eq. (4.18) of [25] wherein inviscid roll wave solutions to the shallow water equations are considered.

**APPENDIX B: LINEAR STABILITY OF THE PAYNE-WHITHAM MODEL CONSIDERED IN SEC. V**

For a right-hand-side forcing function of type (5.1), the constant base state solution to Eqs. (1.1) and (1.2) is given by

$$\rho = \tilde{\rho}, \quad u = \tilde{u}_0 \left( 1 - \frac{\tilde{\rho}}{\rho_M} \right). \quad (B1)$$

Following ideas discussed in Kerner and Konhäuser [8], Kurtze and Hong [15], Helbing [11] and elsewhere, the linear stability of this base state can be explored by introducing perturbation (hatted) quantities, defined such that

$$\rho = \tilde{\rho} + \hat{\rho}, \quad u = \tilde{u}_0 \left( 1 - \frac{\tilde{\rho}}{\rho_M} \right) + \hat{u}, \quad (B2)$$

where  $\hat{\rho}$  and  $\hat{u}$  are expressed in terms of normal modes by

$$\hat{\rho} = \hat{R} e^{ikx + \sigma t} \quad \text{and} \quad \hat{u} = \hat{U} e^{ikx + \sigma t}. \quad (B3)$$

Here  $k$  is the horizontal wave number and  $\sigma$  is the corresponding growth rate. Application of Eqs. (B2) and (B3) into Eqs. (1.1) and (1.2) shows that

$$\begin{bmatrix} \sigma + ik\psi & ik\tilde{\rho} \\ \frac{\tilde{u}_0}{\tau\rho_M} + i\beta'k & \sigma + ik\psi + \frac{1}{\tau} \end{bmatrix} \begin{bmatrix} \hat{R} \\ \hat{U} \end{bmatrix} = \begin{bmatrix} 0 \\ 0 \end{bmatrix}, \quad (B4)$$

where, for notational economy, we have introduced

$$\psi = \tilde{u}_0 \left( 1 - \frac{\tilde{\rho}}{\rho_M} \right), \quad \beta' = \frac{\beta}{\rho_M - \tilde{\rho}}. \quad (B5)$$

Requiring that the determinant of the matrix from Eq. (B4) vanishes shows that

$$\sigma = -ik\psi - \frac{1}{2\tau}(1 + Y), \quad (B6)$$

in which

$$Y^2 = 1 - 4k^2\beta'\tilde{\rho}\tau^2 + 4ik\tilde{u}_0\tau\frac{\tilde{\rho}}{\rho_M}. \quad (B7)$$

Generically,  $Y$  may be written as  $Y = \Lambda_1 - i\Lambda_2$ , where

$$\Lambda_1^2 - \Lambda_2^2 = 1 - 4k^2\beta'\tilde{\rho}\tau^2, \quad (B8)$$

and

$$\Lambda_1 \Lambda_2 = -2k\tilde{u}_0 \tau \frac{\tilde{\rho}}{\rho_M}. \quad (\text{B9})$$

Eliminating  $\Lambda_2$  from Eqs. (B8) and (B9) yields the following polynomial expression:

$$\mathcal{P}(\Lambda_1^2) = \Lambda_1^4 - (1 - 4k^2 \beta' \tilde{\rho} \tau^2) \Lambda_1^2 - 4k^2 \tilde{u}_0^2 \tau^2 \frac{\tilde{\rho}^2}{\rho_M^2} = 0. \quad (\text{B10})$$

Linear stability requires a nonpositive growth rate, i.e.,

$$\text{Real}(\sigma) \leq 0 \Leftrightarrow 0 \leq \Lambda_1^2 \leq 1 \Leftrightarrow \mathcal{P}(1) \geq 0. \quad (\text{B11})$$

From Eq. (B10), the latter condition is satisfied provided

$$\frac{\beta}{\rho_M - \tilde{\rho}} \geq \frac{\tilde{\rho} \tilde{u}_0^2}{\rho_M^2}, \quad (\text{B12})$$

where Eq. (B5) has been employed. Solving this equation for  $\tilde{\rho}$  yields Eq. (5.12), which is the desired result.

- 
- [1] D. Helbing, *Rev. Mod. Phys.* **73**, 1067 (2001).
  - [2] H. J. Payne, *Transp. Res. Rec.* **722**, 68 (1979).
  - [3] L. A. Pipes, *J. Appl. Phys.* **24**, 274 (1953).
  - [4] G. F. Newell, *Oper. Res.* **9**, 209 (1961).
  - [5] W. F. Phillips, *Transp. Plan. Technol.* **5**, 131 (1979).
  - [6] M. J. Lighthill and G. B. Whitham, *Proc. R. Soc. London, Ser. A* **229**, 317 (1955).
  - [7] P. I. Richards, *Oper. Res.* **4**, 42 (1956).
  - [8] B. S. Kerner and P. Konhuser, *Phys. Rev. E* **48**, R2335 (1993).
  - [9] B. S. Kerner and P. Konhuser, *Phys. Rev. E* **50**, 54 (1994).
  - [10] A. Aw and M. Rascle, *SIAM J. Appl. Math.* **60**, 916 (2000).
  - [11] D. Helbing, *Eur. Phys. J.: Appl. Phys.* (to be published); Characteristic speeds faster than the average vehicle speed do not constitute a theoretical inconsistency of macroscopic traffic models.
  - [12] G. B. Whitham, *Linear and Nonlinear Waves* (John Wiley and Sons, Inc., New York, 1974).
  - [13] R. J. LeVeque, *Numerical Methods for Conservation Laws* (Birkhuser Verlag, Basel, Switzerland, 1992).
  - [14] Y. Sugiyama, M. Fukui, M. Kikuchi, K. Hasebe, A. Nakayama, K. Nishinari, S. Tadaki, and S. Yukawa, *New J. Phys.* **10**, 033001 (2008).
  - [15] D. A. Kurtze and D. C. Hong, *Phys. Rev. E* **52**, 218 (1995).
  - [16] L. C. Evans, *Partial Differential Equations: Graduate Studies in Mathematics* (American Mathematical Society, Providence, RI, 1998), Vol. 19.
  - [17] W. Fickett and W. C. Davis, *Detonation* (University of California Press, Berkeley, CA, 1979).
  - [18] D. S. Stewart and A. R. Kasimov, *SIAM J. Appl. Math.* **66**, 384 (2005).
  - [19] A. R. Kasimov, *J. Fluid Mech.* **601**, 189 (2008).
  - [20] F. R. Gilmore, M. S. Plesset, and H. E. Crossley, Jr., *J. Appl. Phys.* **21**, 243 (1950).
  - [21] J. J. Stoker, *Water Waves* (Interscience, New York, USA, 1957).
  - [22] T. S. Komatsu and S. I. Sasa, *Phys. Rev. E* **52**, 5574 (1995).
  - [23] B. S. Kerner, S. L. Klenov, and P. Konhuser, *Phys. Rev. E* **56**, 4200 (1997).
  - [24] C. F. Daganzo, *Transp. Res., Part B: Methodol.* **29**, 277 (1995).
  - [25] R. F. Dressler, *Commun. Pure Appl. Math.* **2**, 149 (1949).
  - [26] N. J. Balmforth and S. Mandre, *J. Fluid Mech.* **514**, 1 (2004).
  - [27] S. K. Chakrabarti, *Theory of Transonic Astrophysical Flows* (World Scientific, Singapore, 1990).
  - [28] D. Elad, R. D. Kamm, and A. H. Shapiro, *J. Fluid Mech.* **203**, 401 (1989).
  - [29] M. Treiber, A. Hennecke, and D. Helbing, *Phys. Rev. E* **59**, 239 (1999).
  - [30] J. J. Monaghan, *Comput. Phys. Commun.* **48**, 89 (1988).
  - [31] P. Lax and B. Wendroff, *Commun. Pure Appl. Math.* **13**, 217 (1960).
  - [32] G. A. Dilts, *Int. J. Numer. Methods Eng.* **44**, 1115 (1999).
  - [33] J. Yu and J. Kevorkian, *J. Fluid Mech.* **243**, 575 (1992).